J. Fluid Mech. (1983), *vol.* 127, *pp.* 185–201
Printed in Great Britain

The stability and disturbance-amplification characteristics of vertical mixed convection flow

By VAN P. CAREY
Department of Mechanical Engineering, University of California, Berkeley, CA 94720

AND BENJAMIN GEBHART
Department of Mechanical Engineering and Applied Mechanics, University of Pennsylvania, Philadelphia, PA 19104

(Received 5 February 1982 and in revised form 21 July 1982)

An experimental and theoretical investigation has been conducted to determine the stability and disturbance-amplification characteristics of the combined forced and free convection flow adjacent to a vertical uniform-heat-flux surface in a uniform free stream. Previous studies of the stability of mixed convection flows have been limited to linear stability analysis of the effect of weak buoyancy on the neutral stability of a stronger forced flow. Here we consider circumstances where forced-convection effects are small compared with buoyancy effects. The flow behaviour is analysed using linear stability theory. The analysis incorporates a new formulation which permits the calculation of amplification contours for a given flow circumstance. The governing equations have been solved numerically to generate stability planes including the neutral curve and constant amplification contours. Stability planes are presented for assisting and opposed flows at Prandtl numbers Pr of 0·733 and 6·7. In air ($Pr = 0{\cdot}733$), the presence of a weak free stream is found to cause the disturbance-amplification rates and the filtered frequency to deviate strongly from those found in purely free-convection flow. In water ($Pr = 6{\cdot}7$), the effect of a free stream is much weaker. In addition, hot-wire and thermocouple measurements of the filtered frequencies and the disturbance-amplitude distributions are presented for aiding mixed convection flow in air. The measurements are found to be in very good agreement with the calculated results of the stability analysis.

1. Introduction

As a consequence of the many studies of transition mechanisms conducted over the past several decades, it is now generally accepted that transition to turbulence in many boundary-layer flows is a consequence of the amplification of initially small disturbances. For both forced-flow boundary layers and vertical natural convection boundary layers, abundant experimental evidence is available which indicates that in the early stages of transition small disturbances may amplify in two-dimensional sinusoidal form. These then initiate a train of events which ultimately convert a laminar flow to turbulence.

Linear stability theory has been the principal tool used to analyse the early stages of instability and disturbance growth in both forced-flow boundary layers and in natural convection boundary-layer flows. For natural convection boundary-layer flows near an isothermal or uniform-heat-flux surface, linear stability theory predicts that a certain narrow band of frequencies will be highly amplified as the disturbances

are convected downstream. Studies by Jaluria & Gebhart (1974), Mahajan & Gebhart (1978) and others have experimentally confirmed that the filtered frequency predicted by linear stability theory also remains dominent during the early stages of transition. In contrast, this type of frequency filtering is not predicted to occur in Blasius flow. Instead, linear theory predicts that all disturbances below a certain frequency level will first amplify and then decay. Lower frequencies begin to amplify farther downstream and amplify more; but they, like higher frequencies, are predicted eventually to decay. A discussion of Blasius flow stability is found in Jordinson (1970). Hence, in Blasius flow the disturbance-amplification characteristics are quite different from those in vertical natural convection boundary-layer flows.

Since small disturbances are found to amplify initially in two-dimensional sinusoidal form in both Blasius flow and in vertical natural convection boundary-layer flows, mixed convection flows along vertical flat surfaces may be expected to have the same characteristics. For assisting mixed convection flows over a vertical surface, Merkin (1969) points out that near the leading edge the flow is mainly forced convection since thermal transport is not yet established. At large downstream distances, the flow behaviour approaches that of purely natural convection flow. Based on these surmises, if the free-stream flow is vigorous enough to be unstable near the leading edge, it is expected that the stability and disturbance-growth characteristics of the flow will resemble those of Blasius flow. If, on the other hand, the free-stream velocity is small, the flow will become unstable further downstream, where its disturbance-amplification behaviour should resemble that of natural convection flow. Hence the stability and disturbance-amplification characteristics of these flows may, in general, depend on the relative importance of buoyancy and free-stream effects.

Laminar mixed convection flows over vertical surfaces commonly occur in the environment and in technical applications. Numerous studies of such flows have appeared in the literature. A brief discussion of past investigations of laminar mixed convection flows over vertical flat surfaces may be found in Carey & Gebhart (1981). Past studies of the stability characteristics of such flows are very sparse. Mucoglu & Chen (1978) have used linear stability theory to analyse the wave instability of mixed convection flow over a vertical isothermal surface. Conditions near the leading edge are considered, where buoyancy effects are small compared with forced-flow effects. The base flow was computed using the local non-similarity method. In the stability analysis, the local non-similarity method was used to include the non-parallel effects of the base flow. Neutral-stability curves are presented for a range of the buoyancy parameter Gr_x/Re_x^2. Both aiding and opposed effects are analysed for values of the Prandtl number of 0·7 and 7·0. For aiding flow it was found that increasing buoyancy stabilizes the flow, while for opposed flow increasing buoyancy has a destabilizing effect.

With these results, it is difficult, for a given flow circumstance, with given values of free-stream velocity, surface temperature and ambient temperature, to extract the x-location of initial instability. This arises because the neutral-stability curves were computed for fixed values of Gr_x/Re_x^2, which is an x-dependent parameter. The formulation used here circumvents this difficulty.

In more recent studies, Chen & Mucoglu (1979) and Chen & Moutsoglou (1979) have analysed the wave instability of mixed convection flow over horizontal and inclined surfaces respectively. Both these studies also consider mixed convection flows in which the buoyancy effects are small compared with forced-flow effects. In both studies neutral stability curves are presented for both aiding and opposed buoyancy effects.

The present analytical and experimental results apply to mixed convection flows in which the effect of the free-stream velocity is small compared with the effect of buoyancy. Linear analysis is used to determine the stability and disturbance-amplification behaviour of mixed convection boundary-layer flow adjacent to a vertical uniform-heat-flux surface. For the relatively small free-stream effects considered here, these flows were found to retain the selective frequency amplification which is characteristic of pure natural convection flows. The experimental measurements of naturally arising disturbance frequencies and disturbance-amplitude profiles support the analytical results.

2. Analysis

The analysis concerns combined forced and natural convection flow adjacent to a vertical uniform-heat-flux surface. The free-stream velocity is assumed to be constant and sufficiently small that near the conditions of first instability it only slightly alters the flow from its purely natural convection behaviour. The present analysis neglects variable-property effects and the viscous dissipation and pressure terms in the energy equation. It incorporates the usual Boussinesq and boundary-layer approximations. With these assumptions, the governing equations for the steady base flow are

$$\frac{\partial u}{\partial x}+\frac{\partial v}{\partial y}=0, \tag{1}$$

$$u\frac{\partial u}{\partial x}+v\frac{\partial u}{\partial y}=g\beta_{\mathrm{t}}(t-t_\infty)+\nu\frac{\partial^2 u}{\partial y^2}, \tag{2}$$

$$u\frac{\partial t}{\partial x}+v\frac{\partial t}{\partial y}=\alpha_{\mathrm{t}}\frac{\partial^2 t}{\partial y^2}, \tag{3}$$

where x is the distance measured vertically upward from the lower edge of the plate, y is the coordinate normal to the surface, t is the temperature and u and v are the velocities in the x- and y-directions respectively. Here g is the acceleration due to gravity, β_{t} is the coefficient of thermal expansion, ν is the kinematic viscosity and α_{t} is the thermal diffusivity. The boundary conditions for the base flow are

$$u=v=0, \quad \frac{\partial t}{\partial y}=\frac{-q}{k} \quad \text{at} \quad y=0, \tag{4}$$

$$u=u_\infty, \quad t=t_\infty \quad \text{at} \quad y\to\infty, \tag{5}$$

where q is the surface heat flux, k is the fluid thermal conductivity, and t_∞ and u_∞ are the ambient temperature and free-stream velocity respectively. The characteristic speed U, length δ, and temperature difference ΔT are defined as

$$U=\frac{\nu G^{*2}}{5x}, \quad \delta=\frac{5x}{G^*}, \quad \Delta T=\frac{q\delta}{k}, \tag{6a}$$

where G^* is related to the Grashof number Gr_x^* as

$$G^*=5(\tfrac{1}{5}Gr_x^*)^{\frac{1}{5}}, \quad Gr_x^*=\frac{g\beta_t q x^4}{k\nu^2}. \tag{6b}$$

The base flow is non-similar. The non-dimensional stream and temperature functions F and H are therefore defined as

$$F(x,\eta) = \psi/U\delta, \tag{7}$$

$$H(x,\eta) = (t-t_\infty)/\Delta T, \tag{8}$$

where $\eta = y/\delta$ is the normalized y-coordinate, and by definition $u = \psi_y$ and $v = -\psi_x$.

As shown by Carey & Gebhart (1981), it is possible to obtain expansions for $F(x,\eta)$ and $H(x,\eta)$ for large downstream distances. Consistent with the parallel-flow and boundary-layer assumptions which will be used in the stability analysis, only the first two terms of these expansions are retained here:

$$F(x,\eta) = F_0(\eta) + \epsilon_M F_1(\eta) + \ldots, \tag{9}$$

$$H(x,\eta) = H_0(\eta) + \epsilon_M F_1(\eta) + \ldots, \tag{10}$$

where

$$\epsilon_M = \frac{Re_x}{(\frac{1}{5}Gr_x^*)^{\frac{2}{5}}}, \quad Re_x = \frac{u_\infty x}{\nu}.$$

Note that increasing the expansion parameter ϵ_M corresponds to increasing forced convection effects. For use in the stability analysis, ϵ_M is written as

$$\epsilon_M = R^*/G^{*\frac{2}{7}}, \tag{11a}$$

where

$$R^* = 5u_\infty\left(\frac{k}{g\beta_t q\nu^2}\right)^{\frac{1}{4}} = \frac{5Re_x}{Gr_x^{*\frac{1}{4}}}. \tag{11b}$$

All the x-dependence of ϵ_M is then contained in the $G^{*\frac{2}{7}}$ factor in (11a). The parameter R^* is a constant for a given flow circumstance. Its magnitude is dependent on the free-stream velocity, the surface heat flux and the properties of the fluid. For a given flow circumstance, increasing downstream distance x corresponds to increasing G^* and decreasing ϵ_M. The parameter R^* is an indicator of the importance of forced-flow effects on the flow as a whole, while $G^{*\frac{2}{7}}$ in (11a) quantifies the variation of forced-flow effects with downstream distance.

Substituting (7) and (8) into (1)–(5), with (9)–(11), yields the following equations and boundary conditions for the base-flow quantities:

$$F_0''' + 4F_0F_0'' - 3F_0'^2 + H_0 = 0, \tag{12a}$$

$$H_0'' + Pr(4F_0H_0' - F_0'H_0) = 0, \tag{12b}$$

$$F_0(0) = F_0'(0) = H_0'(0) + 1 = F_0'(\infty) = H_0(\infty) = 0, \tag{12c}$$

$$F_1''' + F_1F_0'' + 4F_0F_1'' - 3F_0'F_1' + H_1 = 0, \tag{13a}$$

$$H_1'' + Pr(F_1H_0' + 4F_0H_1' + 2H_1F_0' - F_1'H_0) = 0, \tag{13b}$$

$$F_1(0) = F_1'(0) = H_1'(0) = F_1'(\infty) - \tfrac{1}{5} = H_1(\infty) = 0. \tag{13c}$$

In the usual manner for stability analysis, the velocity, temperature and pressure are each assumed to be the sum of a mean and fluctuating component, here designated as barred and primed quantities respectively:

$$u = \bar{u} + u', \quad v = \bar{v} + v', \quad t = \bar{t} + t', \quad p = \bar{p} + p'. \tag{14}$$

The disturbances are assumed to be small and two-dimensional such that the disturbance stream function ψ' and temperature fluctuation t' are postulated as

$$\psi' = U\delta\phi(\eta)\, e^{i(\hat{\alpha}x-\hat{\beta}\tau)}, \tag{15}$$

$$t' = \Delta T s(\eta)\, e^{i(\hat{\alpha}x-\hat{\beta}\tau)}, \tag{16}$$

where by definition $u' = \psi'_y$ and $v' = -\psi'_x$. The functions $\phi(\eta)$ and $s(\eta)$ represent the variation of the disturbance amplitudes across the boundary layer. In general both $\hat{\alpha}$ and $\hat{\beta}$ may be complex. The recent trend in stability analysis is to calculate spatial amplification rates, whereupon $\hat{\alpha}$ is taken to be complex and $\hat{\beta}$ is real. The real part of $\hat{\alpha}$ is the wavenumber and the imaginary part is the spatial (in x) exponential amplification rate. Physical quantities correspond to the real part of complex functions.

The forms for u, v, t and p in (14) are substituted into the complete two-dimensional time-dependent governing equations. After subtracting the base-flow quantities and applying the boundary-layer and parallel-flow assumptions, the x-momentum and y-momentum equations are combined into the vorticity equation to eliminate the pressure terms. Substituting (7), (8), (15) and (16), the following equations for the disturbance-amplitude functions $\phi(\eta)$ and $s(\eta)$ are obtained:

$$(\phi''-\alpha^2\phi)\left(F'-\frac{\beta}{\alpha}\right)-\phi F''' = \frac{1}{i\alpha G^*}(\phi^{\mathrm{iv}}-2\alpha^2\phi''+\alpha^4\phi+s'), \tag{17}$$

$$s\left(F'-\frac{\beta}{\alpha}\right)-\phi H' = \frac{1}{i\alpha G^* Pr}(s''-\alpha^2 s). \tag{18}$$

Here α and β are the non-dimensional complex wavenumber and frequency given by

$$\alpha = \hat{\alpha}\delta, \quad \beta = \hat{\beta}\delta/U.$$

The boundary conditions for a surface of large thermal capacity are

$$\phi(0) = \phi'(0) = s(0) = \phi(\infty) = \phi'(\infty) = s(\infty) = 0. \tag{19}$$

Equations (17) and (18) are the usual Orr–Sommerfeld equations for natural convection flow over a uniform-heat-flux surface. The difference here is that F and H in (9) and (10) are also functions of G^*, through $\epsilon_{\mathrm{M}} = \epsilon_{\mathrm{M}}(R^*, G^*)$. Each physical flow circumstance, with given u_∞ and q, is indicated by a value of R^*. With q and R^* given, each downstream location has a corresponding G^*, which affects the stability of the flow directly as it appears in (17) and (18) and also as it affects F and H through ϵ_{M}. This is more clearly seen if (17) and (18) are written as

$$(\phi''-\alpha^2\phi)\,(F_0'+R^*G^{*-\frac{1}{4}}F_1'-\beta/\alpha)-\phi(F_0'''+R^*G^{*-\frac{1}{4}}F_1''') = \frac{1}{i\alpha G^*}(\phi^{\mathrm{iv}}-2\alpha^2\phi''+\alpha^4\phi+s'), \tag{20}$$

$$s\left(F_0'+R^*G^{*-\frac{1}{4}}F_1'-\frac{\beta}{\alpha}\right)-\phi(H_0'+R^*G^{*-\frac{1}{4}}H_1') = \frac{1}{i\alpha G^* Pr}(s''-\alpha^2 s). \tag{21}$$

This formulation incorporates directly the non-similar base flow in terms of G^*. This makes it possible to calculate the neutral curve and downstream amplification contours for a given flow circumstance, that is, a given R^*.

As discussed by Hieber & Gebhart (1971) and Mahajan & Gebhart (1978), the

boundary-layer approximations employed in both the base-flow and stability equations amount to neglecting terms in the governing equations of $O(G^{*-1})$ and smaller. Hence, the base-flow quantities in (20) and (21) are consistent with the boundary-layer assumptions used here. Equations (20) and (21) constitute a sixth-order linear ordinary differential equation for the disturbance-amplitude distributions $\phi(\eta)$ and $s(\eta)$. The solutions $\phi(\eta)$ and $s(\eta)$ are eigenfunctions for the eigenvalues α and β.

3. Numerical-integration procedure

The sixth-order system of linear homogeneous differential equations (20) and (21) with boundary conditions (19) was solved using the method of Hieber & Gebhart (1971). Since the equations are linear the full solution is written as the sum of three linearly independent solutions

$$\phi = \phi_1 + B_2\phi_2 + B_3\phi_3, \tag{22a}$$

$$s = s_1 + B_2 s_2 + B_3 s_3. \tag{22b}$$

Since this is an eigenvalue problem, the eignefunctions are determined up to a multiplicative constant. Here the magnitude of the disturbance functions has arbitrarily been set by taking the coefficient of ϕ_1 to be 1. The three linearly independent integrals (ϕ_1, s_1), (ϕ_2, s_2) and (ϕ_3, s_3) may be chosen so that their asymptotic solutions, to first order as $\eta \to \infty$, are

$$\phi_1 = e^{-\alpha\eta}, \quad s_1 = 0, \tag{23a}$$

$$\phi_2 = e^{-\alpha_2\eta}, \quad s_2 = 0, \tag{23b}$$

$$\phi_3 = e^{-\alpha_3\eta}, \quad s_3 = (\alpha_3^2 - \alpha^2)\left\{\alpha_3^2 - \alpha^2 + iG^*\left(\beta - \frac{\alpha R^*}{5G^{*\frac{3}{4}}}\right)\right\}\frac{\phi_3}{\alpha_3}, \tag{23c}$$

where

$$\alpha_2 = \left[\alpha^2 - iG^*\left(\beta - \frac{\alpha R^*}{5G^{*\frac{3}{4}}}\right)\right]^{\frac{1}{2}}, \tag{23d}$$

$$\alpha_3 = \left[\alpha^2 - iPrG^*\left(\beta - \frac{\alpha R^*}{5G^{*\frac{3}{4}}}\right)\right]^{\frac{1}{2}}. \tag{23e}$$

As in Hieber & Gebhart (1971), (ϕ_1, s_1), (ϕ_2, s_2) and (ϕ_3, s_3) remain the inviscid, the viscous uncoupled and the viscous coupled integrals respectively.

Equations (20) and (21) with boundary conditions (19) were solved as follows. For specified values of Pr, R^*, β and G^*, a complex value for α was guessed. Using (23) as starting values at some η, the three integrals (ϕ_1, s_1), (ϕ_2, s_2) and (ϕ_3, s_3) were integrated separately across the boundary region using a fourth-order predictor–corrector method. From the values of the integrals at the wall, B_2 and B_3 were determined by the boundary conditions $\phi(0) = 0$ and $\phi'(0) = 0$. The remaining boundary condition, $s(0) = 0$, is satisfied for the given G^* and β only if α takes on a specfic value (eigenvalue). Equations for the α-derivatives were integrated together with each of the three integrals. This determined the α-derivatives of ϕ, ϕ' and s at $\eta = 0$. With $\phi_\alpha(0)$, $\phi'_\alpha(0)$, $s_\alpha(0)$ and the Cauchy–Riemann relations, an improved guess for α was obtained by linear extrapolation. The process was repeated until $|s(0)|$ was sufficiently small, typically less than 10^{-4}.

For convenience, computations were done for specific values of the frequency parameter B^* rather than β, where

$$B^* = \beta G^{*\frac{1}{2}} = 2\pi f(g\beta_t q/k)^{-\frac{1}{2}}. \tag{24}$$

Note that B^* is proportional to physical frequency f, and independent of G^* in any given flow. Hence constant frequency lines are horizontal on the (B^*, G^*)-plane. To obtain values of G^* and B^* on the neutral curve ($\alpha_i = 0$), the computational procedure described above was iterated for successive G^*, with B^* fixed, until $|\alpha_i| \leqslant 10^{-5}$.

Note that in (15) and (16) the amplitudes of ψ' and t' change as a result of two effects. The spatial growth due to the unstable nature of the flow is associated with the exponential terms in (15) and (16). ψ' and t' will grow if the real part of $\hat{\alpha}$ is positive. In addition, the base-flow quantities U, δ and ΔT all grow with increasing x, which tends to increase the amplitudes of ψ' and t'. The disturbance growth rate associated with the exponential terms is therefore a measure of how fast the disturbance amplitude changes relative to the base-flow quantities. A 'neutrally damped' disturbance is growing with downstream distance at the same rate as the base-flow quantities.

As any given disturbance component of frequency f is convected downstream from a position corresponding to a value of G^* on the neutral curve G^*_N, to an arbitrary location $x = L$ corresponding to G^*_L, the ratio A_L/A_N of the disturbance amplitudes at the two locations is given by

$$\frac{A_L}{A_N} = e^A, \quad A = -\frac{1}{4}\int_{G^*_N}^{G^*_L} \alpha_i \, dG^*, \tag{25}$$

where the integration is at constant B^* on, for example, figure 1 where the neutral curves are shown as $A = 0$, for $Pr = 0{\cdot}733$ with $R^* = 0$ and 20. To determine the A-contours, for any given values of Pr and R^*, the corresponding neutral curve is used as the starting point for any frequency B^*. The selected value of B^* is held constant while integrating downstream. For the chosen value of G^*, (24) is used to determine β. The procedure described above is then used to determine the value of α corresponding to G^* and β. Marching along at constant B^*, in small steps of G^* (typically 5), the accumulated amplification is computed using the simple trapezoidal rule to approximate the integral in (25) for A. This procedure was repeated for the number of physical frequency paths required to determine constant-A contours, as plotted in figure 1, for $A = 1$, 2, 4 and 6.

The disturbance velocity and temperature distributions are written in terms of the solutions ϕ and s from (15) and (16) as

$$u' = U' \cos\left[\frac{\alpha x}{\delta} - \frac{\beta U \tau}{\delta} + \theta_u\right], \tag{26}$$

$$v' = V' \sin\left[\frac{\alpha x}{\delta} - \frac{\beta U \tau}{\delta} + \theta_v\right], \tag{27}$$

$$t' = T' \cos\left[\frac{\alpha x}{\delta} - \frac{\beta U \tau}{\delta} + \theta_t\right], \tag{28}$$

where

$$U' = U[(\phi'_r)^2 + (\phi'_i)^2]^{\frac{1}{2}}, \quad \theta_u = \arctan\frac{\phi'_i}{\phi'_r}, \tag{29}$$

$$V' = U[\alpha_r^2 + \alpha_i^2]^{\frac{1}{2}}[(\phi_r)^2 + (\phi_i)^2]^{\frac{1}{2}}, \tag{30a}$$

$$\theta_v = \arctan\frac{\alpha_i}{\alpha_r} + \arctan\frac{\phi_i}{\phi_r}, \tag{30b}$$

$$T' = \Delta T[s_r^2 + s_i^2]^{\frac{1}{2}}, \quad \theta_t = \arctan\frac{s_i}{s_r}. \tag{31}$$

The subscripts r and i denote the real and imaginary parts, respectively. Since the disturbance equations are linear and homogeneous, the absolute magnitudes of the disturbances cannot be determined. The disturbance-amplitude distributions U', V' and T' are therefore normalized by their maximum values across the boundary region. This yields

$$\frac{U'}{U'_{\max}} = \frac{\{(\phi'_{\mathrm{r}})^2 + (\phi'_{\mathrm{i}})^2\}^{\frac{1}{2}}}{\{(\phi'_{\mathrm{r}})^2 + (\phi'_{\mathrm{i}})^2\}^{\frac{1}{2}}_{\max}}, \tag{32}$$

$$\frac{V'}{V'_{\max}} = \frac{\{(\phi_{\mathrm{r}})^2 + (\phi_{\mathrm{i}})^2\}^{\frac{1}{2}}}{\{(\phi_{\mathrm{r}})^2 + (\phi_{\mathrm{i}})^2\}^{\frac{1}{2}}_{\max}}, \tag{33}$$

$$\frac{T'}{T'_{\max}} = \frac{\{(s_{\mathrm{r}})^2 + (s_{\mathrm{i}})^2\}^{\frac{1}{2}}}{\{(s_{\mathrm{r}})^2 + (s_{\mathrm{i}})^2\}^{\frac{1}{2}}_{\max}}. \tag{34}$$

4. Numerical results

Figure 1 compares the downstream amplification with G^* for air, $Pr = 0{\cdot}733$, at $R^* = 0$ and 20. Recall that $R^* = 0$ is pure natural convection and $R^* = 20$ corresponds to aiding mixed convection flow with $Re_x = \frac{4}{5}G^{*-\frac{5}{4}}$. Since the results are plotted in terms of B^*, constant-frequency lines are horizontal. The magnitude of R^* is restricted to less than 20 for $Pr = 0{\cdot}733$, so that the free-stream velocity u_∞ does not exceed the maximum natural convection velocity at the nose of the neutral curve. This ensures the accuracy of the base-flow perturbation solution.

Several important results are apparent in figure 1. First, the downstream amplification is much less for $R^* = 20$ than for $R^* = 0$. In addition, far downstream, at G^* near 600, the band of most rapidly amplified frequencies appears slightly higher for $R^* = 20$ than for $R^* = 0$. At lower G^*, near $G^* = 350$, the selectivity is less sharp for $R^* = 20$ than for $R^* = 0$. For $R^* = 20$, lower-frequency disturbances, near $B^* = 0{\cdot}8$, are most strongly amplified, whereas farther downstream, at $G^* = 600$, frequencies near $B^* = 1{\cdot}6$ are amplified most rapidly. For $R^* = 0$, the band of favoured frequencies varies less strongly with G^*. However, the neutral curves for the two different conditions do not differ significantly. The shift in the constant-A curves indicates that an assisting free stream has a stabilizing effect.

Mixed convection flow circumstances may also arise in which the forced-flow and buoyancy effects are opposed. Carey & Gebhart (1981) have pointed out a few weakly opposed flow circumstances for which the perturbation analysis, used here for the base flow, may be a reasonably accurate model. Hence, we have also applied the stability analysis to weakly opposed flows for which $R^* < 0$. In figure 2 the stability planes for $R^* = 0$ and -10 are compared, also for $Pr = 0{\cdot}733$. It can be seen there that the effect on disturbance amplification is the opposite of that for aiding flow. Although the neutral curve is again about the same, the amplified band is shifted downward. Also, the downstream amplification is much higher for $R^* = -10$. An opposed free stream has a sharply destabilizing effect on the flow.

For $Pr = 6{\cdot}7$, characteristic of water, the magnitude of R^* is restricted to less than 8, to ensure that the free-stream velocity is less than the peak natural convection velocity for conditions along the neutral curve. Figure 3 compares the constant-amplification curves obtained for $R^* = -4$, 0 and 8 at $Pr = 6{\cdot}7$. The free-stream velocity is seen to have very little effect on the disturbance-growth characteristics. The neutral curve and amplification curves show very little change. Flows in air apparently are much more sensitive to the presence of a free-stream velocity than flows in water.

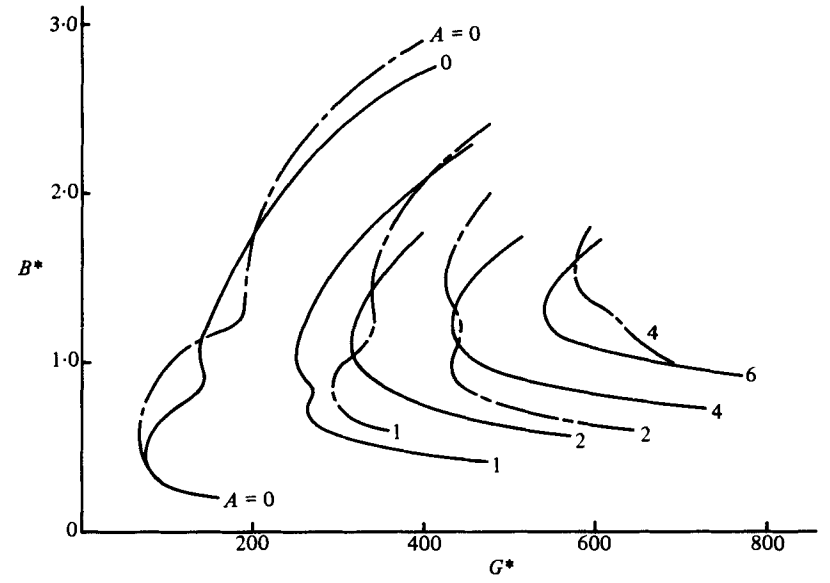

FIGURE 1. Amplification-rate contours corresponding to $R^* = 0$ (—) and 20 (— — —) for $Pr = 0{\cdot}733$.

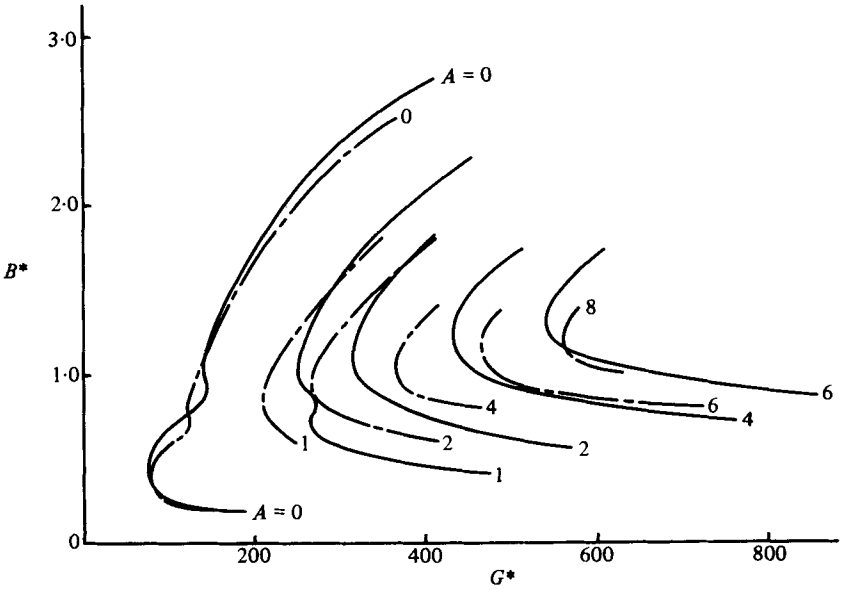

FIGURE 2. Amplification-rate contours corresponding to $R^* = 0$ (——) and -10 (— — —) for $Pr = 0{\cdot}733$.

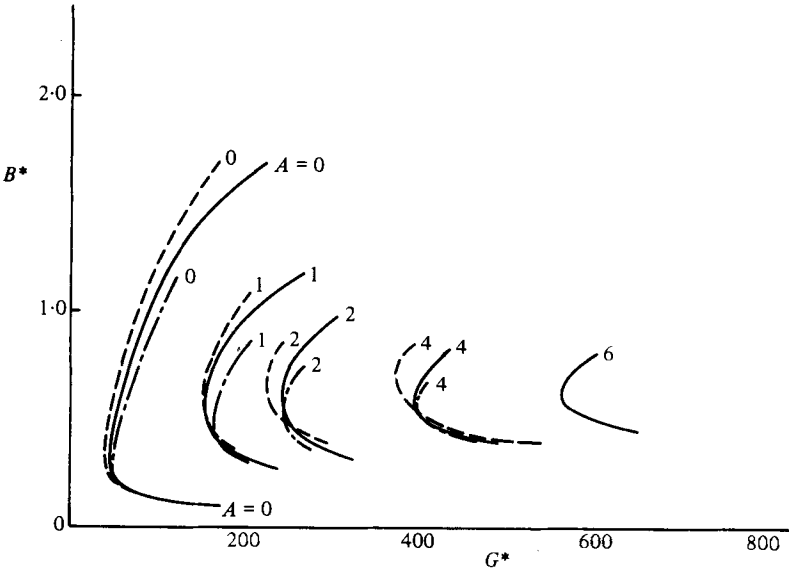

FIGURE 3. Amplification-rate contours corresponding to $R^* = -4$ (– – –), 0 (——) and 8 (– – – –) for $Pr = 6{\cdot}7$.

5. Experiments in air

To assess the accuracy of the analysis presented in the previous section, experimental measurements were made in the mixed convection flow adjacent to a vertical uniform-heat-flux surface in air. The experimental system is shown in figure 4. The experiments were conducted in a cylindrical test section of inside diameter 33·7 cm and height 76·2 cm. The heated surface was formed by stretching a 15 cm wide piece of 0·0127 mm thick Inconel 600 foil in a special support fixture. The jaws at the top of the fixture were spring-loaded so that they exerted an upward force on the foil. The foil was looped around an aluminium support covered with plastic tape. This support resisted the upward pull of the jaws and thereby pulled the foil tight. A 0·64 cm thick piece of foam insulation was inserted between the two sections of foil, so that at steady state all heat dissipated by the foil was transferred outward to the surrounding air. The resulting assembly formed a surface, heated on both sides, 15 cm wide, 40 cm high and 0·64 cm thick, with a front and back surface of the Inconel foil and an interior of foam insulation. The lower aluminium support provided a smooth leading-edge configuration. Passing electric current through the foil provided a uniform-heat-flux surface condition.

Prior to the experiments, the surface was aligned vertically, with the leading edge horizontal, using a plumb line and level. Air flow was supplied to the test section by a line from a compressed-air storage tank. The storage tank was maintained at about 7 atm pressure by a system which compressed and dehumidified the air. Air from the storage tank was sent through a pressure regulator, a critical orifice flowmeter and then into the test section. The system had a peak flow capacity of about 0·7 m^3/s at 1 atm pressure. This amounted to a peak mean velocity of 7·5 cm/s in the test section. By maintaining critical flow conditions at the orifice in the orifice meter, the flow through the test section was a function only of the pressure upstream of the meter. The pressure there was held with $\pm 0{\cdot}07$ atm (± 7 kPa) by the pressure

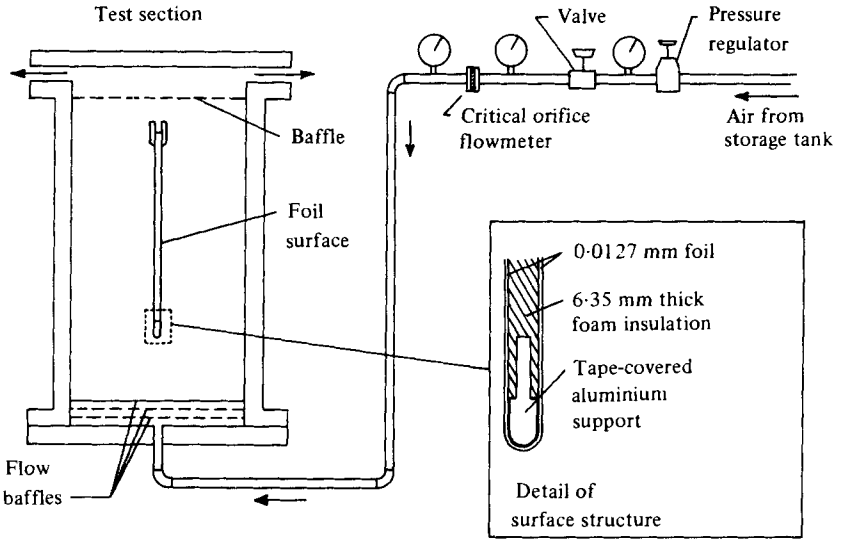

FIGURE 4. System used for mixed convection experiments.

regulator. The flow through the test section was thereby held constant within $\pm 0{\cdot}05$ cm/s. Measurements indicated that the temperature of the air supplied to the test section did not vary by more than $\pm 0{\cdot}05$ °C during a test. These tolerances could be held for as long as 45 minutes, despite cycling of the compressor to maintain the storage tank pressure. The air flow rate was also measured with the critical orifice meter, as a rough check of the hot-wire measurements of the mean flow in the test section.

Large-pressure-drop baffles were inserted at the top and bottom of the test section to ensure uniform flow distribution over the test section. Hot-wire measurements across the test section, made before inserting the surface, indicated that the flow was uniform to within $\pm 0{\cdot}10$ cm/s. During the experiments, the variation of the core velocity with vertical location was found to be negligible. The usual acceleration of the core flow which occurs in the entrance of a pipe was not appreciable because acceleration of the fluid by buoyancy, near the surface, approximately compensates for the deceleration of fluid by shear in the boundary layer along the test-section wall. The support structure for the surface was designed to minimize drag, and the structural members were far away from the heated surface.

A regulated power supply was used to provide electrical power to the foil. During the experiment, the voltage was measured across the foil using a Hewlett-Packard 3465B digital multimeter. The voltage was also measured across a Leeds & Northrup 0·01 Ω, 100 A standard shunt in series with the foil, to determine the foil current. The foil current, and the voltage drop, were used to calculate the heat flux from the surface.

Velocity measurements were made using a Disa 55M01 constant-temperature hot-wire anemometer with a Disa 55P14 miniature probe. The output from the anemometer was measured with a Hewlett-Packard 3455A digital voltmeter. The hot-wire probe was L-shaped so that the wire was upstream of the probe support. This minimized probe-support interference. The probe was calibrated in air using the test rig of Shaukatullah (1977). This is a modification of the earlier apparatus of Dring

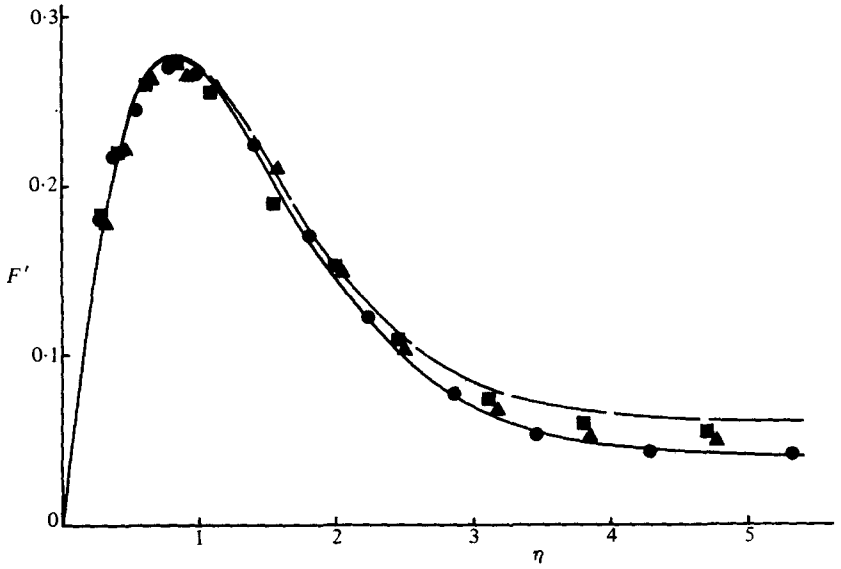

FIGURE 5. Measured mean-velocity profiles in mixed convection flow along a vertical uniform-heat-flux surface in air. The values of (R^*, G^*, ϵ_M) and the corresponding symbols for the experimental data are (15, 319, 0·20) (●); (20, 351, 0·24) (▲); (22, 350, 0·27) (■). Also shown are the calculated laminar profiles for $\epsilon_M = 0{\cdot}20$ (——) and 0·30 (– – –).

& Gebhart (1969). The probe was calibrated at an overheat ratio of 1·6 for velocities up to 40 cm/s. The method described by Mahajan (1977) was used to correct the hot-wire output for the effect of varying ambient temperature. A discussion of this correction method may also be found in Carey (1981).

The boundary-layer temperature measurements were made using a 0·0254 mm copper–constantan thermocouple. The two thermocouple leads were horizontal and parallel to the foil for about 0·8 cm on each side of the junction. In this arrangement, the wire lay essentially along an isotherm in the thermal layer, reducing the conduction loss in the leads. These leads then passed through a pair of 1·0 mm hollow glass tubes which were attached to a support outside the boundary region. This support also held the hot-wire probe and the surface probe. The latter, a 1·5 mm copper rod, was used to locate the surface. The foil location was determined by connecting the surface probe through a resistance meter to the foil. The circuit was completed when the probe contacted the foil, causing the resistance reading to drop from an open circuit to some finite value.

The relative positions of the thermocouple and hot-wire sensors, with respect to this surface probe, were determined from an enlarged photograph of the assembly. The hot-wire sensor, thermocouple junction and surface probe were in the same horizontal plane. The ambient air temperature in the tank was measured using a 0·0127 cm copper–constantan thermocouple. An ice bath was used as a reference for both thermocouples. The output from the thermocouples was measured using a Hewlett–Packard 3465B multimeter as a voltmeter.

The probe array was remotely traversed normal to the foil, in the boundary layer, using a Disa 55H01 traversing mechanism. This was driven by a Disa 55C01 stepper motor, which was remotely controlled by a Disa 55B01 sweep drive unit. The output level corresponding to any given probe position was displayed with high accuracy

on the three-digit mechanical counter of the sweep drive unit. The probe could be accurately moved in steps of 0·203 mm. The distance of the probe from the leading edge was measured accurately before putting the assembly in the tank.

The thermocouple leads, the coaxial hot-wire cable and all the other electrical leads were taken out of the test section through sealed fittings in the side and top of the tank.

After turning on the air supply and applying the foil current, the flow was allowed about 2 min to reach steady state, for each test. Thermocouple and hot-wire readings were then taken at a number of points across the boundary layer. All measurements were taken at a single downstream location 31·4 cm above the lower edge of the surface. This was about 9 cm below the upper edge. For this apparatus this was the farthest downstream location at which data could be taken without interference from the trailing edge. The maximum downstream distance was chosen to provide as much distance as possible for disturbances to amplify in the flow. This maximized the relative accuracy of the disturbance-amplitude measurements, given the finite resolution of the probes and the size of the apparatus.

In each experiment, the convection heat flux was determined from the temperature measurements in the flow close to the surface, and from the power input to the foil. As described in Carey (1981), the temperature measurements were used to correct for the weak effect of thermal radiation from the surface.

For the apparatus described above, it was found that, for G^* values above about 320 and at moderate flow rates, very small disturbances present in the free-stream flow were amplified in the boundary layer. The resulting outputs from the hot-wire and thermocouple probes were recorded using a Beckman analog chart recorder and a Hewlett-Packard 3455A digital voltmeter. The analog outputs indicated that the disturbances were almost purely sinusoidal. From the recorded output the disturbance frequencies and the profiles of disturbance and mean quantities across the boundary region, were determined.

Figure 5 shows the measured mean-velocity profiles for $(R^*, G^*, \epsilon_M) = (15, 319, 0{\cdot}20), (20, 351, 0{\cdot}24)$ and $(22, 350, 0{\cdot}27)$. The estimated uncertainty in the data is $\pm 4\,\%$ of the peak velocity for the velocity measurements and $\pm 2\,\%$ of the peak temperature for the temperature measurements. Also shown in figure 5 are the calculated laminar profiles for $\epsilon_M = 0{\cdot}20$ and $0{\cdot}30$. These measurements show no significant deviation from the calculated laminar variation. Figure 6 compares measured mean and calculated temperature profiles, again with excellent agreement. As assumed in the stability analysis, at this early, and linear, stage of the transition process, the mean flow deviates very little from steady laminar flow behaviour.

Figures 7 and 8 show, as points, the measured disturbance velocity and temperature data respectively for $(R^*, G^*, \epsilon_M) = (20, 351, 0{\cdot}24)$ and $(22, 350, 0{\cdot}27)$. The data shown in these figures are the largest oscillatory disturbances observed at each location during about 60 s of recorded thermocouple and hot-wire output. Hence, they represent the most highly amplified disturbances in the flow. The 60 s interval was chosen as a consistent means of comparison. Results obtained for successive 60 s intervals, and in repeated tests, were consistent to within about 10 %. The data in figures 7 and 8 are therefore believed to be representative for these flows. The disturbance-velocity data was obtained by correcting the hot-wire output for temperature effects using the method of Mahajan (1977).

Also shown in figures 7 and 8 are the computed disturbance and phase profiles for $B^* = 0{\cdot}8$ and $1{\cdot}6$ for $(R^*, G^*, \epsilon_M) = (20, 350, 0{\cdot}24)$. The comparison of these data with

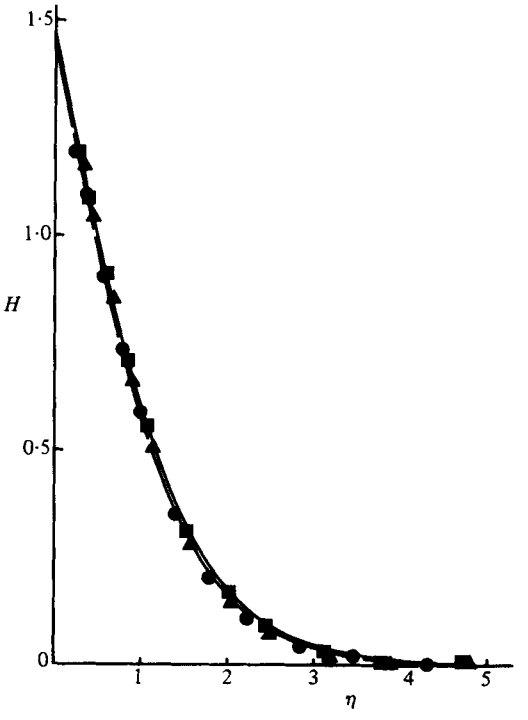

FIGURE 6. Measured mean-temperature profiles in mixed convection flow along a vertical uniform-heat-flux surface in air. The values of (R^*, G^*, ϵ_M) and the corresponding symbols for the experimental data are (15, 319, 0·20) (●); (20, 351, 0·24) (▲); (22, 350, 0·27) (■). Also shown are the calculated laminar profiles for $\epsilon_M = 0$ (——) and 0·30 (– – –).

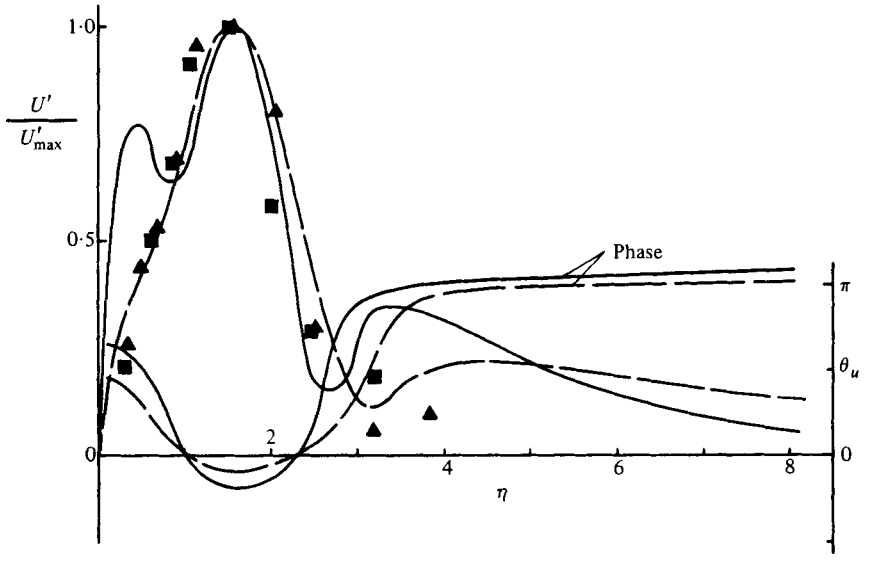

FIGURE 7. Measured velocity-disturbance profiles for (R^*, G^*, ϵ_M) = (20, 351, 0·24) (▲) and (22, 350, 0·27) (■). Also shown are the theoretical profiles for (R^*, G^*, ϵ_M) = (20, 350, 0·24) for $B^* = 0·8$ (– – –) and 1·6 (——).

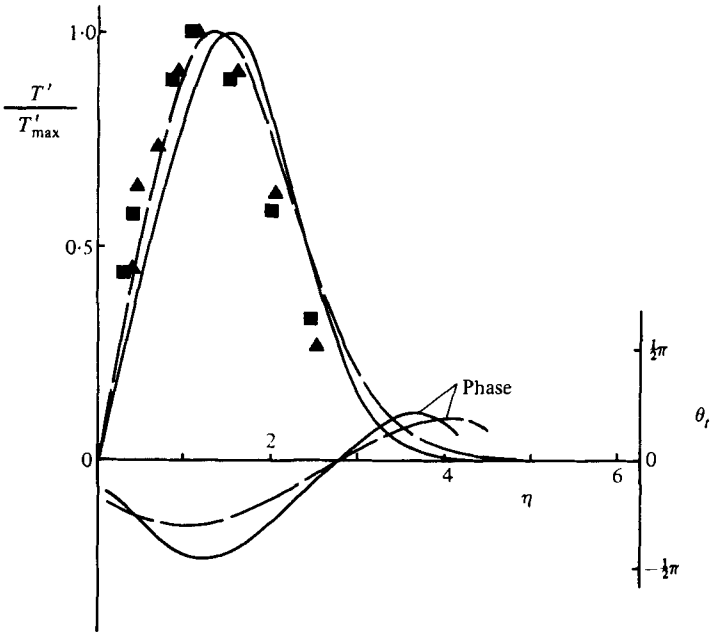

FIGURE 8. Measured temperature-disturbance profiles for $(R^*, G^*, \epsilon_M) = (20, 351, 0{\cdot}24)$ (▲) and $(22, 350, 0{\cdot}27)$ (■). Also shown are the theoretical profiles for $(R^*, G^*, \epsilon_M) = (20, 350, 0{\cdot}24)$ for $B^* = 0{\cdot}8$ (– – –) and $1{\cdot}6$ (——).

U'/U'_{max} is appropriate since the analysis predicts that $|v'|/|u'|$ is small over much of the boundary layer. The curves for $B^* = 0{\cdot}8$ and $1{\cdot}6$ are shown because they span the range of most highly amplified frequencies at $G^* = 350$, $R^* = 20$ (see figure 1). It is seen in figures 7 and 8 that the data agree more closely with the distributions for $B^* = 0{\cdot}8$. This is not surprising since these data represent the largest disturbance seen at each transverse (y) location. As seen in figure 1, the most highly amplified disturbances (largest A) at $G^* = 350$, $R^* = 20$ occur near $B^* = 0{\cdot}8$. At these moderate values of G^*, for $R^* = 20$, lower frequencies are more highly amplified than the higher frequencies that eventually dominate farther downstream.

The measured frequencies for a range of R^* and G^* are shown in figure 9. For each of the experiments, a range of frequencies was found in the analog data. The two frequencies which were found most often in the analog data for each condition are plotted in figure 9 along with the stability planes for $R^* = 0$ and 20. It can be seen that the theoretical curves predict that, for R^* near 20 and $G^* = 350$, disturbances with frequencies corresponding to B^* between $0{\cdot}8$ to $1{\cdot}6$ will be most highly amplified. The frequencies encountered most often in the experimental data do correspond to values of B^* in this range, as seen in figure 9. The experimental observations are therefore consistent with the selective amplification predicted by the analysis.

6. Conclusions

Linear stability analysis has been applied to mixed convection flow adjacent to a vertical uniform-heat-flux surface in a weak uniform free stream. This new formulation makes it possible to calculate the neutral curve and constant-amplification curves for a given physical flow circumstance, i.e. fluid, free-stream velocity and surface heat

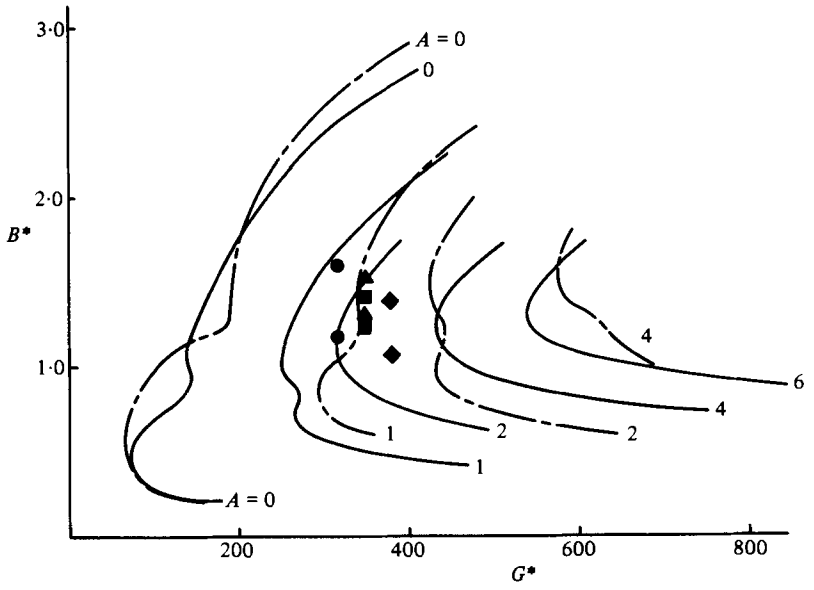

FIGURE 9. Characteristic frequencies observed in mixed convection flow along a vertical uniform-heat-flux surface in air. The experimental conditions are $(R^*, G^*, \epsilon_M) = (15, 319, 0{\cdot}20)$ (●); (22, 350, 0·27) (■); (20, 351, 0·24) (▲); (16, 380, 0·19) (◆). Also shown are the calculated amplification rate contours for $R^* = 0$ (——) and 20 (— — —).

flux. In gases it was found that the disturbance amplification rates in mixed convection flow differed strongly from those in purely natural convection flow. The amplification rates are lower with an assisting free stream and higher with an opposed free stream. Hence an aiding free stream has a stabilizing effect for gases, while an opposed free stream tends to destabilize the flow. An aiding free-stream flow causes an upward shift in the band of favoured frequencies for gases. The opposite effect was found for an opposed free-stream flow. For $Pr = 0{\cdot}733$, from $R^* = 0$ to 20, the value of B^* corresponding to the centre of the band of favoured frequencies changed from about 1·3 to 1·6. For $R^* = -10$, the favoured band centre shifted downward to about 1·1. In water, the effect of an aiding or opposed free stream is almost negligible. However, in both air and water, the flow retained the preferential amplification of a narrow band of frequencies which is characteristic of purely free-convection flow.

Experimental measurements in aiding mixed convection flows in air confirm the behaviour calculated from linear stability analysis. In the early stages of disturbance amplification, the measured mean velocity and temperature profiles deviate very little from those predicted for laminar flow. The measured disturbance-amplitude distributions agreed well with those predicted by the analysis. They appear to confirm the predicted preferential amplification of lower frequencies, near $B^* = 0{\cdot}8$, at $G^* = 350$, for $R^* = 20$. The observed frequencies in the hot-wire and thermocouple output are all near the band of preferred frequencies predicted by the analysis. On the whole, the experimental results imply that, in the early stages of disturbance amplification, linear stability theory provides reasonably accurate information about disturbance behaviour in mixed convection flows in air.

The first author would like to acknowledge graduate fellowship support from the Graduate School at the State University of New York at Buffalo. The authors also wish to acknowledge support for this work by the National Science Foundation under research grant ENG77-21641.

REFERENCES

CAREY, V. P. 1981 Transport in vertical mixed convection flows and natural convection flows in cold water. Ph.D. dissertation, State University of New York at Buffalo.

CAREY, V. P. & GEBHART, B. 1981 Transport at large downstream distances in mixed convection flow adjacent to a vertical uniform-heat-flux surface. Submitted to *Int. J. Heat Mass Transfer.*

CHEN, T. S. & MOUTSOGLOU, A. 1979 Wave instability of mixed convection flow on inclined surface. *Numer. Heat Transfer* **2**, 497–509.

CHEN, T. S. & MUCOGLU, A. 1979 Wave instability of mixed convection flow over a horizontal flat plate. *Int. J. Heat Mass Transfer* **22**, 185–196.

DRING, R. P. & GEBHART, B. 1969 Hot wire anemometer calibration for measurements at very low velocity. *Trans. A.S.M.E.* C: *Heat Transfer* **91**, 241–244.

HIEBER, C. A. & GEBHART, B. 1971 Stability of vertical natural convection boundary layers: some numerical solutions. *J. Fluid Mech.* **48**, 625–646.

JALURIA, Y. & GEBHART, B. 1974 On transition mechanisms in vertical natural convection flow. *J. Fluid Mech.* **66**, 309–337.

JORDINSON, R. 1970 The flat plate boundary layer. Part 1. Numerical integration of the Orr–Sommerfeld equation. *J. Fluid Mech.* **43**, 801–811.

MAHAJAN, R. L. 1977 Higher-order effects, stability and transition in vertical natural convection flows. Ph.D. Dissertation, Cornell University.

MAHAJAN, R. L. & GEBHART, B. 1978 High-order approximations to the natural convection flow over a uniform-flux vertical surface. *Int. J. Heat Mass Transfer* **21**, 549–556.

MAHAJAN, R. L. & GEBHART, B. 1979 An experimental determination of transition limits in a vertical natural convection flow adjacent to a surface. *J. Fluid Mech.* **91**, 131–154.

MERKIN, J. H. 1969 The effect of buoyancy forces on the boundary-layer flow over a semi-infinite vertical flat plate in a uniform free stream. *J. Fluid Mech.* **35**, 439–450.

MUCOGLU, A. & CHEN, T. S. 1978 Wave instability of mixed convection flow along a vertical flat plate. *Numer. Heat Transfer* **1**, 267–283.

SHAUKATULLAH, H. 1977 An experimental investigation of the natural convection boundary layer over a uniform flux inclined surface. Ph.D. Dissertation, Cornell University.